JACS
JOURNAL OF THE AMERICAN CHEMICAL SOCIETY

Article

pubs.acs.org/JACS

Oxidative Dehydrogenation of Ethane on Dynamically Rearranging Supported Chloride Catalysts

Christian A. Gärtner,[†] André C. van Veen,[†,‡] and Johannes A. Lercher*[,†]

[†]Department of Chemistry and Catalysis Research Center, Technische Universität München, Lichtenbergstraße 4, 85747 Garching, Germany

[‡]School of Engineering, The University of Warwick, Library Road - Office A421, Coventry CV4 7AL, U.K.

Supporting Information

ABSTRACT: Ethane is oxidatively dehydrogenated with a selectivity up to 95% on catalysts comprising a mixed molten alkali chloride supported on a mildly redox-active Dy_2O_3-doped MgO. The reactive oxyanionic OCl^- species acting as active sites are catalytically formed by oxidation of Cl^- at the MgO surface. Under reaction conditions this site is regenerated by O_2, dissolving first in the alkali chloride melt, and in the second step dissociating and replenishing the oxygen vacancies on MgO. The oxyanion reactively dehydrogenates ethane at the melt−gas phase interface with nearly ideal selectivity. Thus, the reaction is concluded to proceed via two coupled steps following a Mars-van-Krevelen-mechanism at the solid−liquid and gas−liquid interface. The dissociation of O_2 and/or the oxidation of Cl^- at the melt−solid interface is concluded to have the lowest forward rate constants. The compositions of the oxide core and the molten chloride shell control the catalytic activity via the redox potential of the metal oxide and of the OCl^-. Traces of water may be present in the molten chloride under reaction conditions, but the specific impact of this water is not obvious at present. The spatial separation of oxygen and ethane activation sites and the dynamic rearrangement of the surface anions and cations, preventing the exposure of coordinatively unsaturated cations, are concluded to be the origin of the surprisingly high olefin selectivity.

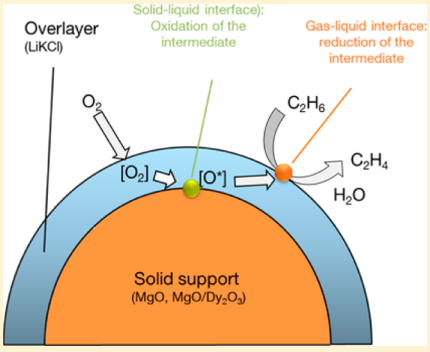

INTRODUCTION

The oxidative dehydrogenation (ODH) of ethane is conceptually a selective route from ethane to ethene, which replaces the external energy input in the generation of ethene by coupling it to the oxidation of hydrogen. The economic feasibility of the route, however, necessitates a very high olefin selectivity, as it competes as a process with ethane steam cracking. To be viable, the process must avoid not only the losses by total oxidation, but also the formation of aromatic byproducts.[1]

Oxidative dehydrogenation requires the activation of both reactants, O_2 and ethane. It is usually assumed to occur via the formation of the reactive species either by redox[2] or radical[3] chemistry. This is followed by the abstraction of two H atoms and the formation of a C-C double bond upon desorption. As the formed π-bond interacts strongly with coordinatively unsaturated metal cations, it tends to react further on many redox active catalysts. Total oxidation of ethane and ethene is also more exothermic than ODH, thus being thermodynamically favored. An ideal catalyst must therefore be selective for C-H bond breaking but not for oxygen insertion, the reaction that eventually leads to the total oxidation of the carbon atom to which the oxygen is attached.[4] Such a catalyst should also be able to adsorb the paraffin more strongly than the olefin. Ethene desorption must be fast and the readsorption of ethene, mainly facilitated by coordinatively unsaturated metal cations on surfaces, should be minimized.

A recent review of the main classes of catalysts considered for ethane ODH indicates that for most catalysts the first C-H bond activation either via single electron transfer (i.e., radical) or involving paired electrons (i.e., redox) is rate determining.[4] While in nearly all the cases, the initial CH bond is broken homolytically, catalysts that operate via a Mars-van-Krevelen-redox mechanism exhibit, in general, high ethene selectivity, while catalysts supporting free radical pathways yield high selectivity to CO_x. The factors governing activity and selectivity include the metal−oxygen bond strengths in oxide catalysts, the specific atomic arrangement of the active sites, the concentration of these sites, as well as the ease of desorption and readsorption of ethene.[4]

Supported alkali chloride catalysts have been reported to show a surprisingly high olefin selectivity in the oxidative dehydrogenation of ethane. The excellent selectivity of such catalysts has been associated with the fact that the catalysts are supported alkali or alkaline earth chlorides that are molten and therefore dynamically rearrange under reaction conditions.[5,6] Ethene selectivity in the ODH of ethane has been reported to exceed 90%. The low density of sites and the facile desorption of ethene seem to be especially relevant factors. The density of sites is low, as the active species are concluded to be dissolved in the melt and homogeneously distributed, making it less likely

Received: June 8, 2014

   dx.doi.org/10.1021/ja505411s | J. Am. Chem. Soc. XXXX, XXX, XXX−XXX

that ethene formed reacts again with such sites. In addition, the molten overlayer provides a dynamically rearranging surface, which is able to minimize the readsorption of ethene, as the chloride melt termination does not allow a long exposure of metal cations to the gas phase. Because activity and selectivity critically depend on the nature and concentration of these dynamically forming active sites, we decided to explore this catalytic chemistry mechanistically, and to study the concentration and dynamic genesis of the active sites under reaction conditions.

For supported alkali chlorides, two different mechanistic hypotheses have been presented. The first proposes the transient formation of OCl^- as catalytically active species, the ODH reaction taking place at the surface of the overlayer.[6] The second suggests the formation of the redox pair Li_2O/Li_2O_2 as active species, which is modified and protected by Cl^- anions.[7] However, both hypotheses have not been substantiated and quantified experimentally. It is reported that alkali chlorides are most effective, if they are used in eutectic compositions, providing faster access to a supported liquid salt. With LiCl as one component, the second can be a different alkali or an alkaline earth chloride.[5,6] Decreasing the melting point of the eutectic compared to pure LiCl results in an increasing selectivity toward ethene, but also decreasing activity. In this study, we have chosen Li-K-Cl in eutectic composition as our model system, since it leads to the catalysts with the highest olefin selectivity reported so far.[6] Additionally, the Li-free eutectic system (Na-Cs)Cl was studied to probe the necessity of the presence Li^+ cations for selective catalysis, aiming to develop a comprehensive mechanistic model, which addresses elementary steps and distinguishes between the mechanistic hypotheses. This holds especially true for the role of the support, while various overlayer compositions have already been studied.[6] The activation of O_2 and ethane has been addressed using transient kinetic studies, implemented in step experiments, which additionally allow the quantification of the O_2 and ethane uptakes. Temperature programmed isotopic exchange experiments enable the quantification of the oxygen dissociation of both support and catalyst, providing important information about the oxygen dissociation step.

RESULTS AND DISCUSSION

Role of Cations and Chloride for the Oxidative Dehydrogenation of Ethane. Figure 1 compiles reaction data for two different eutectic overlayers (Li-K-Cl, mp = 353 °C, Na-Cs-Cl mp = 486 °C) on $MgO+Dy_2O_3$. The rates of ODH markedly exceeded those of total oxidation on both catalysts, i.e., the selectivity to ethene varied between 93% and 100% for Li-K-Cl and between 86% and 94% for Na-Cs-Cl. The pre-exponential factors for the total oxidation were by far lower than the preexponential factors for ODH, indicating only a very small concentration of unselective sites. This difference in the preexponential factors makes the variations in the apparent activation energy less relevant for the activity and selectivity. It is interesting to note that the preexponential factor for CO_2 formation was higher in the case of Na-Cs-Cl, indicating that with larger cations (60% Cs^+ in the case of Na-Cs-Cl, 42.5% K^+ in the case of Li-K-Cl) a higher degree of total oxidation was observed. Because both catalysts had similar activities, it is conclusively demonstrated that the redox pair Li_2O/Li_2O_2 is not essential for ODH of alkanes. In turn, as chloride is the common component in both catalysts (besides the support, which is concluded not to be exposed to the gas phase), the catalytic activity is concluded to involve Cl.

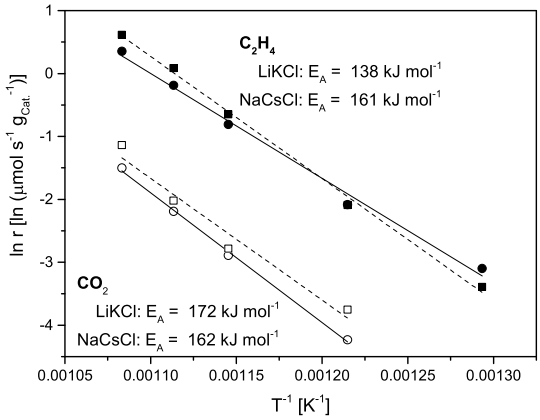

Figure 1. ODH and side reactions: ●,○:Li-K-Cl/MgO + Dy_2O_3 (entry 5, Table 3), ■,□: Na-Cs-Cl/MgO + Dy_2O_3 (entry 10, Table 3); 0.3 g catalyst, WHSV = 0.8 h^{-1} to 2.0 h^{-1}, $P_{O2} = P_{Ethane}$ = 80 mbar.

Impact of the Nature and Thickness of the Chloride Overlayer. As the chloride anion plays a key role in the ODH of ethane on supported alkali chloride catalysts, the influence of its concentration has been quantitatively explored.

A series of catalysts with different molar ratios between the chloride overlayer (LiCl/KCl in eutectic composition[5,6]) and the support (physical mixture of MgO as main support component and Dy_2O_3 as an additional component minor component, i.e., dopant, present as small particles on the surface of MgO) were tested for their activities and surface properties. The Supporting Information (SI) (Figure S1) includes an in situ X-ray diffraction analysis of Li-K-Cl/MgDyO. It is shown that the oxidic support and the chloride overlayer remain in different crystalline phases at ambient temperature and do not form a mixed crystalline phase. Figure S2a (SI) shows the specific surface areas of the catalyst as functions of the molar overlayer fractions ($N_{overlayer}/(N_{overlayer} + N_{support})$).

Table 1 reports the theoretical film thicknesses, for the assumption that the surface area of the support is 69 $m^2\ g^{-1}$ (fresh support) and for the assumption that the surface area of the support is 33 $m^2\ g^{-1}$, i.e., the specific surface area after removal of all chloride layers.

Table 1. Estimated Average Chloride Layer Thicknesses (assumptions: pores are not filled, densities of LiCl and KCl at 20°C)

sample no.	overlayer [mol%]	estimated film thickness for 68 $m^2\ g^{-1}$ [nm]	calculated film thickness for 33 $m^2\ g^{-1}$ [nm]
1	1.3	0.1	0.2
2	3.4	0.3	0.6
3	5.6	0.6	1.2
4	10.7	1.1	2.3
5	19.2	2.2	4.6
6	32.2	4.4	9.2
7	41.7	6.6	13.8

While the pure support had a surface area of 68 $m^2\ g^{-1}$, the addition of the minor overlayer of 1.3 mol % alkali chlorides decreased it to only 12 $m^2\ g^{-1}$. The addition of more chloride resulted in a further, but slower, decrease to 5 $m^2\ g^{-1}$ at a molar

dx.doi.org/10.1021/ja505411s | J. Am. Chem. Soc. XXXX, XXX, XXX−XXX

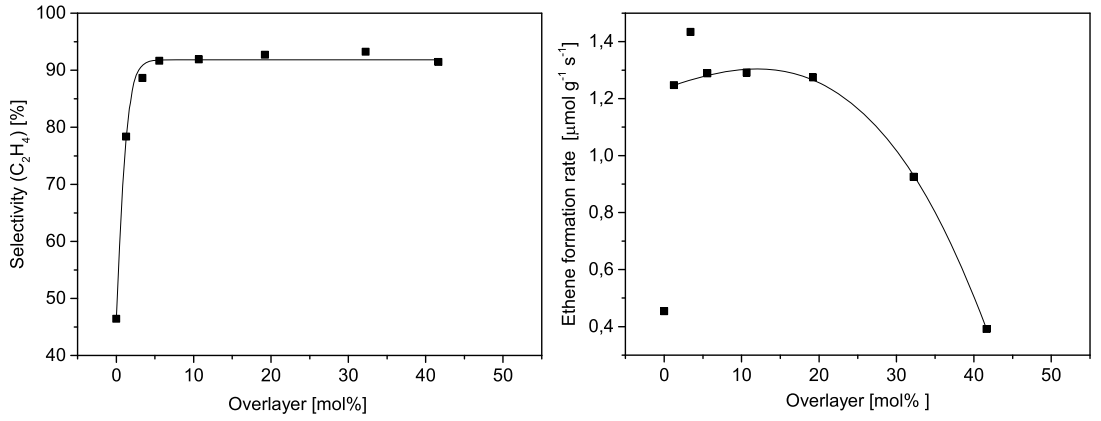

Figure 2. Activities of catalysts with different support/overlayer molar ratios. (LiKCl/MgO + Dy_2O_3, T = 625 °C, WHSV = 0.8 h^{-1}, P_{total} = 1 bar, p_{Ethane} = p_{O2} = 70 mbar; for conversions see Figure S3 of the Si.)

overlayer concentration of 32%. While we assume for these calculations that pore blocking or pore filling did not occur, we think that in reality a fraction of pores will be only partly filled with chloride.

Table S1 of the SI shows the cumulative pore volume of the different samples. Thus, the real film thickness might be greater on average than ideally expected but also widely varying as clearly shown by the transmission electron microscopy graph in Figure S4 of the SI. Obviously, the film thicknesses measured in the example by HAADF-TEM are significantly higher than the calculated film thicknesses compiled in Table 1. In addition to the heterogeneity, this suggests that the chloride layer must have induced significant sintering of the support.

To test this hypothesis, a catalyst (composition according to entry 6 in Table 3) was treated with water in an ultrasonic bath after calcination to wash off the chloride layer. Subsequent BET analysis showed a specific surface area of 33 m^2 g^{-1}, indicating chloride-induced sintering of the oxide support. However, as about half of the specific surface area and the pore volume were restored, we conclude that part of the pores were blocked but not filled. The average nominal overlayer thicknesses of the catalysts (without considering pore blockage) for this specific surface area of the support are also compiled in Table 1.

Figure 2 presents the formation rates and selectivities of catalysts with different overlayer molar fractions. The MgO + Dy_2O_3 support had modest reactivity and selectivity. This is consistent with the literature reporting moderate olefin selectivities in ODH for oxides of alkaline earth and rare earth metals.[3] Poor selectivity of these oxides resulted from facile formation of alkyl radicals that tend to be easier fully oxidized either at the oxide surface[2] or in the gas phase subsequent to their desorption.[3]

Addition of the smallest increment of chloride almost doubled the ODH selectivity and increased the rate normalized to the catalyst weight. The addition of more chloride resulted in a further increase in activity and alkene selectivity, reaching an asymptotic value of around 93% selectivity. The high activity and selectivity was achieved once an average full layer of the alkali chloride was formed. Ethene formation rates tripled upon the initial addition of chloride, suggesting either a boost of activity by chloride or the generation of new sites.

A plateau in ethene productivity was observed as the concentration of active sites increased continuously followed by a decrease in catalytic activity at higher chloride loadings. The catalyst with the thickest overlayer (around 40 mol % overlayer) showed only 30% of the ODH rate compared to the maximum. The addition of increasing concentrations of chloride is concluded to cover the support, blocking first pores of the support, followed by the formation of islands of melt at the outer surface of the support and eventually covering it completely. Apparently, very low concentrations of chloride loaded (see entries 2 and 3 in Table 3) do not prevent the exposure of unselective sites on the supports. Only if a thicker continuous layer is established are the unselective sites covered and the molten overlayer, illustrated by the transmission electron microscopy graph (Figure S4 of the SI), formed.

The increase (and later) decrease of the catalytic activity as a function of the loading with chloride is concluded not to be caused by changes in the support surface (the specific surface area dropped upon addition of chloride) but by the generation of new active sites in the presence of the chloride overlayer. The decrease in activity at higher chloride loadings is attributed to diffusional constraints. Thus, the chloride overlayer is hypothesized to generate a new type of site catalyzing the relatively fast and selective formation of ethene from ethane via ODH. The decrease of the activity with higher chloride loading is concluded to be a consequence of the combination of decreasing specific surface area (after the overlayer has been established) and the complex reaction mechanism shown below. The linear decrease of the rate as a function of the square root of the chloride overlayer thickness suggests that diffusion limitations of the oxidizing species could be the cause for the decreasing reaction rate (Figure S5 of the SI). As will be demonstrated below, the oxidation of Cl^- at the surface of the support has one of the lowest forward rate constants. As the dissolution of O_2 in the molten chloride is quasi-equilibrated and because the outer surface hardly varies with the thickness of the overlayer (Figure S2a of the SI), the concentration of hypochlorite anions in that layer and, hence, on its surface is concluded to decrease. This decrease together with the lower specific surface area must lead to a lower rate in turn.

Table 2 summarizes activation energies and pre-exponential factors of catalysts with different chloride loadings (graphical determination see Figure S7 of the SI).

The bare support (MgO + Dy_2O_3) showed similar activation energies and pre-exponential factors for ODH and side reactions. The addition of chloride (even in low concentrations) resulted in a drastic increase in the activation energies and pre-exponential factors for both reactions. Activation energies of ODH were in the same range (approximately 140

dx.doi.org/10.1021/ja505411s | J. Am. Chem. Soc. XXXX, XXX, XXX−XXX

Table 2. Activation Energies and Pre-exponential Factors of ODH and Total Oxidation Reactions of Catalysts with Different Chloride Concentrations (WHSV = 1.6 h^{-1}, P_{ges} = 1 bar, p_{Ethane} = p_{O2} = 70 mbar)

	ethene formation		CO_x formation	
overlayer/ mol%	E_A/kJ mol^{-1}	A/−	E_A/kJ mol^{-1}	A/−
0	109	1.5×10^6	104	1.7×10^6
5.6	142	2.1×10^8	201	3.9×10^{10}
10.7	143	2.8×10^8	209	1.2×10^{11}
19.2	142	1.9×10^8	192	1.3×10^{10}
32.3	134	5.2×10^7	186	2.00×10^9
41.6	135	2.3×10^7	178	1.3×10^9

kJ mol^{-1}) for all chloride-containing catalysts, slightly decreasing with high loadings (in agreement with influence of diffusion of active species in the layer). The very high values of the apparent activation energies for the total oxidation (approximately 180−200 kJ mol^{-1}) together with the high pre-exponential factors suggest that the main reason for the high selectivity to ethene lies in the energetic blocking of total oxidation. The consistently higher preexponential factor suggests in turn that the transition state for total oxidation is much looser than the transition state for ODH. A recent contribution by Chin et al. suggests that the high apparent energies of activation together with the high preexponential factor point to radical reactions.[8]

The low solubility of organic molecules in the chloride melt makes it unlikely that ethane diffuses through the chloride layer to the redox active support surface to react, because such low solubility would lead to severe diffusion limitations under practical conditions. Thus, the question arises at this point whether a part of the redox active support is dissolved in the chloride melt and acts as a distinct redox site at the liquid−gas interface. The presence of dissolved support in the melt has been probed by washing the chloride from the catalyst with water and analyzing the removed phase by chemical analysis (ICP-OES). The results proved the quantitative absence of cations from the support (Mg^{2+}, Dy^{3+}) in the chloride melt and the stoichiometry of chloride anions and alkali cations. Thus, we conclude that the chloride overlayer does not change in composition during catalysis and that oxidic or chloride species of the support anions do not exist at the surface of the chloride overlayer. This does not rule out the presence of, for example, very small equilibrium concentrations MgO support in a LiCl−KCl eutectic melt at 873 K, which have been measured potentiometrically to be about 10^{-7}. [9]

Full coverage of the catalyst support can be confirmed by findings of Kumar et al, who showed in situ Raman measurements of LiKCl/MgO + Dy_2O_3 at different temperatures. Typical peaks of Dy_2O_3 (382, 471, and 525 cm^{-1}) completely disappeared at a temperature of 500 °C, indicating that the whole support is covered by chloride at this temperature.[5]

Considering these facts and especially the low solubility of organic reactants in the chloride melt, we conclude at this point that the ODH reaction takes place at the gas−alkali chloride interface and involves Cl-containing species. At least for the catalysts with higher chloride loading, which show the best performance, the redox active sites of the support are not exposed to the gas-phase reactants. A reaction test with only SiC reported in Figure S6 of the SI, showing that gas phase reactions contribute less than 3% of the total rate.

Elementary Steps of the Oxidation Reaction. To follow the C−H bond and O_2 activation, transient step experiments were performed to quantify the uptakes of both reactants by the catalyst. The catalyst was flushed with He for 15 s after a 45-min exposure to an O_2-containing He stream for 45 min and prior to reaction with 10% ethane in He. Figure 3a presents the gas concentrations in the effluent.

After equilibrating the catalyst with O_2, ethene formation persisted for approximately 20 min (Figure 3a), showing that

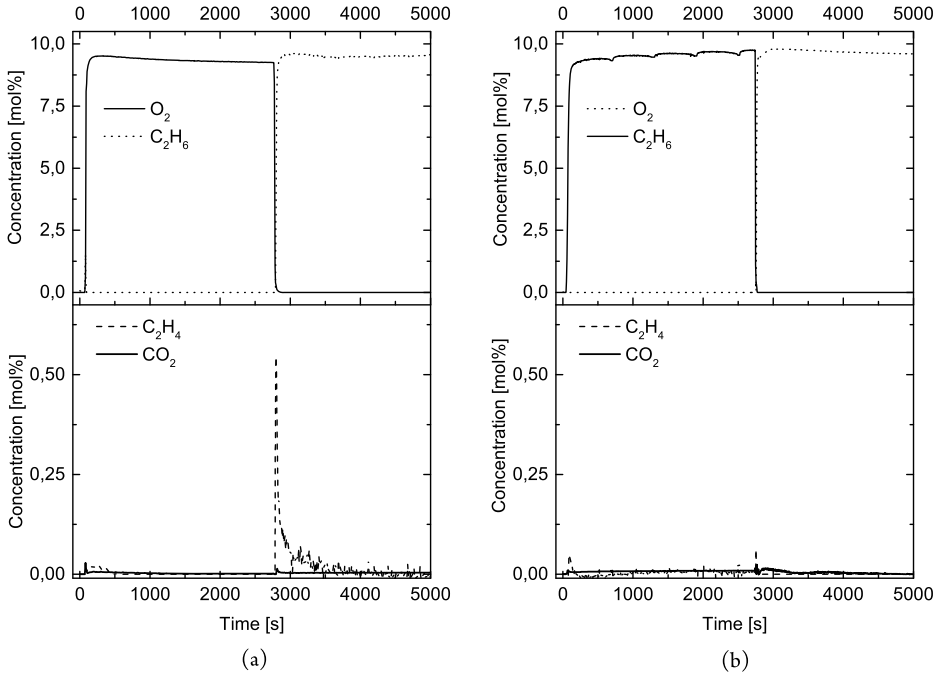

Figure 3. Step experiment at 625 °C on LiKCl/MgO + Dy_2O_3. (Catalyst according to entry 5 in Table 3.) (a) Step from 10% O_2 to 10% C_2H_6. (b) Step from 10% C_2H_6 to 10% O_2.

dx.doi.org/10.1021/ja505411s | J. Am. Chem. Soc. XXXX, XXX, XXX−XXX

the ODH active oxidizing species formed by contact with O_2 were retained in the melt. The persistence of the ethene formation without O_2 feed thus eliminates the possibility that the radical gas phase or surface radical reaction are the catalytically active species, because such radical intermediates tend to be quenched rapidly[8] and would not be expected to be stable after 1200 s. Remarkably, CO or CO_2 were not observed in this step experiment, indicating that the reactive intermediate is ideally selective for the ethene formation and does not catalyze total oxidation of ethene or ethane. A similar experiment was performed, feeding the reactants in reverse order (Figure 3b). Ethene was not detected, demonstrating that the catalyst did not retain ethane. This can be rationalized by the high polarity of the melt causing a low affinity for nonpolar alkanes. Therefore, we conclude that the conversion of ethane to ethene occurs at the surface of the melt, although the O_2 activation and reaction with Cl^- occurs in the bulk phase of the overlayer or on the interface between melt and the molten overlayer.

More information on the O_2 activation was obtained from step experiments at various temperatures. The O_2 uptake increased with temperature as shown in Figure 4a.

The increase of the concentration of O_2, which has reacted to form the oxidizing species, with increasing temperature, shows that O_2 uptake is an activated process, likely involving an endothermic step in the reactive dissociation of O_2.

The values reported in Figure 4a were the maximum capacity of O_2 uptake in the form of the catalytically active intermediate.

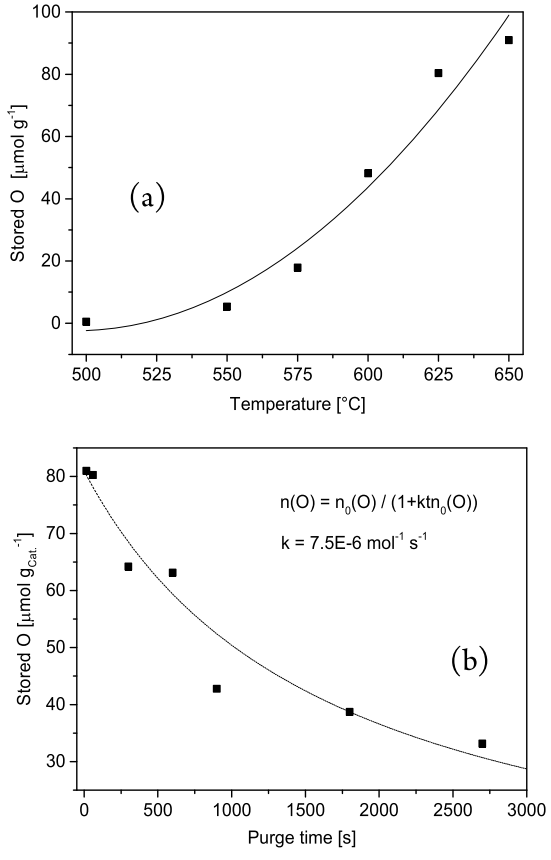

Figure 4. (a) Dependence of O_2 uptake on temperature (oxygen loading time: 45 min; purge time: 0.25 min; (b) Dependence of stored oxygen on purge time (T = 625 °C). (Catalyst according to entry 5 in Table 3.)

An experiment starting under steady state conditions, but with an abrupt stop of O_2 feed (see SI Figure S8) shows that a lower concentration of active intermediate was present in the molten phase under steady state conditions. In order to approximate the rates of the formation of the O−Cl oxidizing intermediate, a step experiment with a short O_2 exposure (1 min) was performed at various temperatures. The results are compiled in Figure S9 of the SI.

The activation energy of the O_2 activation step is higher than the activation energy for the overall ODH. Therefore, we conclude that O_2 is activated in an endothermic step and that the active oxygen oxidizes Cl^- in an exothermic step, forming the active oxidizing species for the ODH, i.e., most likely OCl^-.

The stability of the O−Cl intermediate was probed by additional step experiments with a variable inert purge period between O_2 and ethane exposures. The results are presented in Figure 4b. The concentration of activated O decreased with increasing He purge duration. The decay of the stored O can be described with a second-order kinetics. This indicates that the depletion process follows a bimolecular recombination, and in turn this suggests that the disproportionation has been the rate-determining step, for which the apparent energy of activation of 216 kJ/mol has been determined (Figure S9 of the SI). O_2 was not be detected via MS during the inert purge period. We conclude that the release rate was too small to be able to detect the traces of O_2 released.

Reaction Pathways of the ODH and Side Reactions. Having established that it is possible to generate an oxidizing species (e.g., the hypochlorite anion) that can be stored and reduced, we used the changes in the concentration of isotopes of the reactants (steady state transient kinetic analysis (SSTIKA)) to estimate the rate constants of the individual steps and the evolution of the products ethene and CO_2. Krypton was added as a tracer to monitor the exact signal of the step switch between $^{16}O_2$ and $^{18}O_2$ during steady state ODH reaction with unchanged ethane conversion. Figure 5 shows the responses to the O_2 switch on the product CO_2 and H_2O and on O_2 per se.

By varying the reaction temperature, the overall concentration of the reactive intermediates and conversion rates of oxygen-containing intermediates varied drastically. As expected, the concentration of O_2 decreased with increasing temperature because of increasing O_2 conversion levels of the gas mixture, but eventually the concentrations of $^{16}O_2$ and $^{18}O_2$ were nearly identical at steady-state conditions before and after the step. In contrast, the concentrations of H_2O and CO_2 increased with reaction temperature in accordance with the higher reaction rates at higher temperatures. While the formation of ^{16}O containing CO_2 disappeared eventually, $H_2{}^{16}O$ remained to be significant even after long time on stream, in concentration levels that were proportional to the reaction rates of ODH. Thus, we conclude that the chloride melt must contain a certain concentration of water under steady state conditions. While present, that concentration cannot be quantified. After replacing $^{16}O_2$ by $^{18}O_2$ in a step function, unconverted $^{16}O_2$ disappeared quickly, replaced by $^{18}O_2$, which reached the steady-state concentration asymptotically in a timespan that was shorter for higher temperatures. After the switching, $^{16}O^{18}O$ reached a maximum soon after the step, slowly decreasing thereafter (even at 650 °C it took 1000 s until the last trace of ^{16}O had disappeared). As long as this species is produced, both oxygen isotopes are present in an exchangeable form at the solid−liquid interface.

dx.doi.org/10.1021/ja505411s | J. Am. Chem. Soc. XXXX, XXX, XXX−XXX

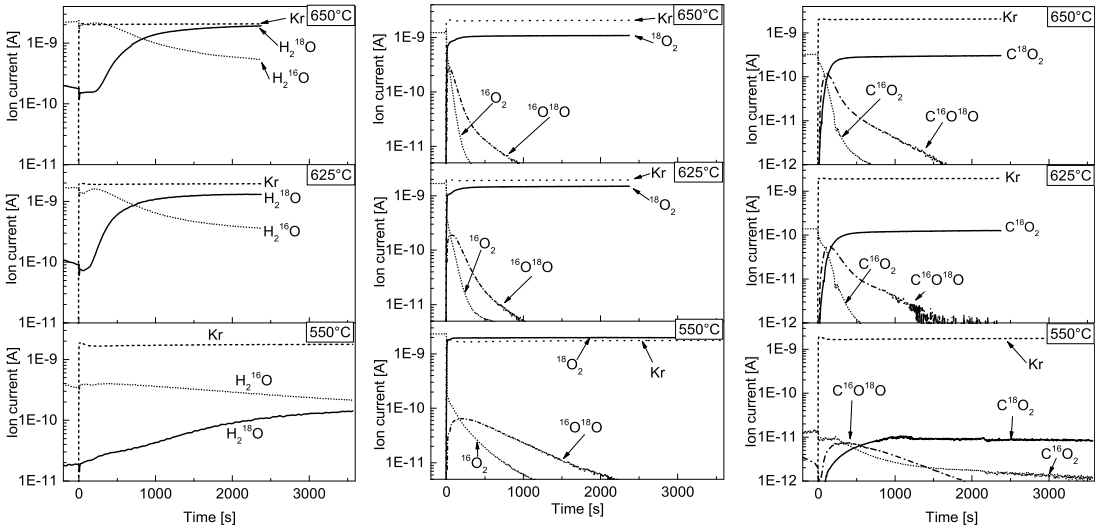

Figure 5. SSITKA results at 550, 625, and 650 °C

The behavior of water mainly produced by the ODH reaction was different. At the lowest temperature, the exchange between $H_2{}^{16}O$ and $H_2{}^{18}O$ was very slow. After 60 min $H_2{}^{16}O$ was still the dominant species. At 625 and 650 °C, the transition from unlabeled to labeled H_2O was faster, $H_2{}^{18}O$ becoming the main product after 15 min. There was an induction period of about 5 min at 650 °C during which only $H_2{}^{16}O$ was formed. This implies that only ^{16}O reactive species were at the surface of the melt and available for reaction with the ethane. It could suggest that the formation of the oxidizing species is slow and competes with O_2 exchange and/or that diffusion of the oxidizing species from the support−liquid interface to the surface of the melt is significant and may influence the overall reaction rate.

Also for CO_2 a similar behavior was observed, including a maximum in the rate of formation of the isotopically mixed product. The time on stream until the last trace of ^{16}O containing CO_2 was detected had been by far longer than the time $^{16}O^{18}O$ was observed. This points either to a retention of CO_2 on the catalyst or to differences in the reactivities along the pathways to form O_2 and CO_2.[10]

Experiments To Elucidate the Critical Individual Reaction Steps. *Experiments with C_2D_6.* The activation of the first ethane C−H bond is the rate-determining step for most catalytic oxidations[11] and for most ODH catalysts (e.g., vanadium oxide-based catalysts[12]). We compared ODH reaction rates for hydrogenated and perdeuterated ethane to quantify the kinetic isotope effect (KIE) for LiKCl/MgO + Dy_2O_3 (Figure 6a). Ethene formation rates vary in dependence on the feed (reflected in the pre-exponential factors). However, the difference is low compared to other ODH catalysts, which show a kinetic isotope effect.[12] Figure 6b presents the experimentally determined ratio of the ethene formation rates of undeuterated and perdeuterated ethane compared to the ratio of rates for a scenario in which the C−H bond activation would be rate determining. The ratio varies with temperature but remained well below the values for a KIE in which C−H bond activation is rate determining. Thus, we conclude that the cleavage of the first C−H bond does not determine the overall rate with the supported chloride catalysts.

Because the reaction rate ratios of the undeuterated and perdeuterated ethane were around 1.2, we conclude that hydrogen is still involved in the rate-determining step, for example in the formation of surface hydroxy or alkoxy species as intermediate products, as also observed with other ODH catalysts.[13]

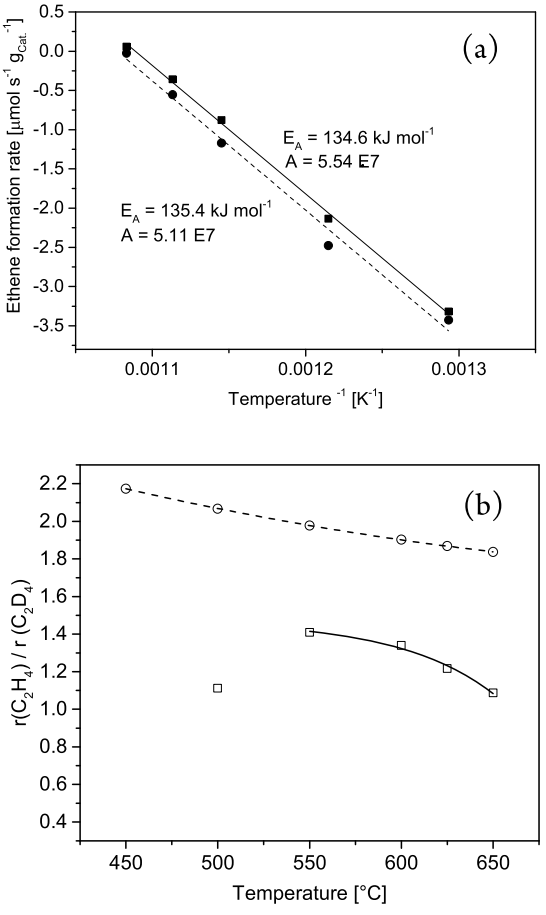

Figure 6. Catalyzed conversion of deuterated and undeuterated ethane. (a) Comparison between ethene productivities for C_2H_6 (■) and C_2D_6 (●) as reactants; (b) experimental ratio of C_2H_4 and C_2D_4 production rates (□), calculated value for the case of a kinetic isotope effect (○)

dx.doi.org/10.1021/ja505411s | J. Am. Chem. Soc. XXXX, XXX, XXX−XXX

Knowing that the O_2 activation is involved in the rate-determining step, we would like to probe this further by comparing supports of different O_2 isotope exchange capacity, as we have concluded that the support is critically participating in the overall reaction.

Influence of the Support Properties. Having established that the surface of the molten chloride phase is the location of the catalytic activation of ethane and that the concentration of oxidizing species determines the overall rate of reaction, the extent to which the redox properties of the support influence this catalytic chemistry is probed. This was done by exploring two oxide supports (bare MgO and ZnO) having less pronounced redox properties, while maintaining identical loadings of LiCl/KCl in the eutectic composition as well as a constant ratio of the support and the overlayer. To rule out trivial coverage effects, the specific surface areas of the supports have been thermally adjusted by sintering MgO (Table S2 of the SI).

Figure 7 shows the activities of catalysts with different supports. Despite similar chloride loadings MgO showed a much higher reactivity than ZnO. The chemical properties of the supports drastically affected the catalytic activities although the supports are covered with the melt and not exposed to the gas phase. The variations in the catalytic properties were mostly related to the differences in the pre-exponential factor, while the activation energies were quite similar. Because of the similarity of the apparent energies of activation we assume that the differences lie in the steady-state concentration of oxidizing species generated at the support−melt interface. We hypothesize that a more redox-active support will generate a larger concentration of oxidizing species (presumably OCl^-).

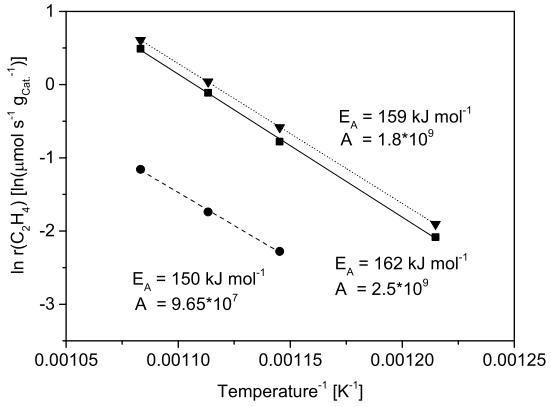

Figure 7. Activities of Li-K-Cl- catalysts with different supports (▼: MgDyO (entry 5 in Table 3); ■: MgO sintered at 900 °C (entry in Table 3); ●: ZnO (entry 9 in Table 3))

As the O_2 dissociation has been concluded to be involved in the rate-determining step we probe another side of this reaction by exploring isotope scrambling of $^{16}O_2$ and $^{18}O_2$.

A stream containing both O_2 isotopes ($^{16}O_2$ and $^{18}O_2$) was passed over the catalyst while the temperature was increased linearly and the formation of $^{16}O^{18}O$ was followed. This allowed the exploration of the temperature dependence of the O_2 dissociation rates for MgO, MgDyO, and ZnO (Figure 8).

As expected, the formation rate of $^{16}O^{18}O$ increased exponentially with temperature. The formation of the isotopically mixed O_2 asserts that O_2 was dissociated and recombines. The much higher rate found with the MgO-based catalysts and of the higher apparent energy of activation of that process

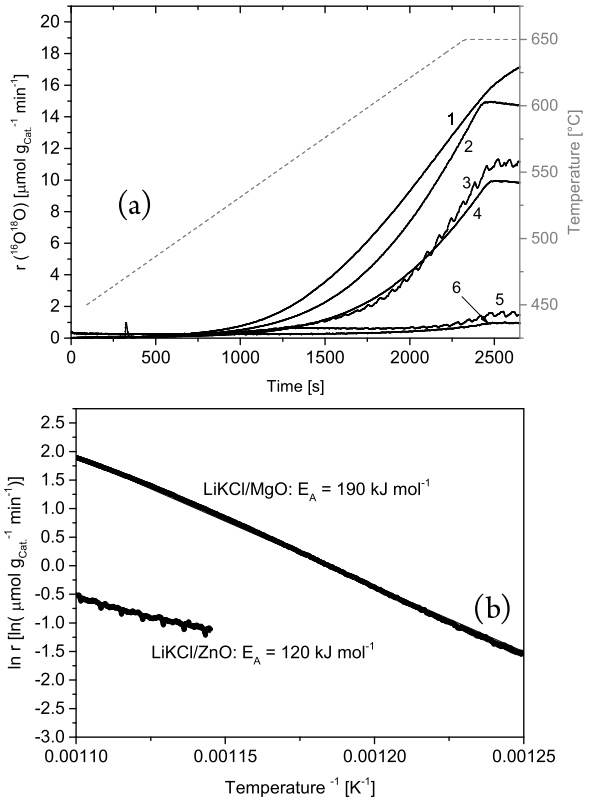

Figure 8. (a) TPIE experiments with different supports and the corresponding LiKCl-coated catalysts (1: MgO + Dy_2O_3; 2: LiKCl/MgO + Dy_2O_3, 3: MgO, 4: LiKCl/MgO, 5: ZnO, 6: LiKCl/ZnO) (b) Arrhenius plot of **4** and **6**.

(Figure 7) suggests that for ZnO the concentration of sites is much lower than for the other two oxides. The addition of Dy leads to higher rates of oxidative dehydrogenation of ethane (Figure 8), which is attributed to the higher reducibility of Dy_2O_3, which leads in turn to a higher rate of formation of the reactive chloride intermediate and to a higher oxygen storage capacity compared to that of MgO.

The activity in the isotope scrambling paralleled the reaction rates in steady state ODH experiments, for which the ranking of the catalytic activity of the materials was identical to isotope scrambling rates reported here.

It should be noted in passing that a corresponding experiment with a mixture of C_2H_6 + C_2D_6 did not lead to isotopically mixed ethane, demonstrating that the hydrocarbons do not reversibly dissociate CH bonds at the catalyst surface, generating a concentration of surface-bound H or D which would permit kinetically significant scrambling. Feeding only $^{18}O_2$ to MgO- and ZnO-based catalysts, which were heated to reaction temperature in He flow without being exposed to $^{16}O_2$ (Figure S10 of the SI), resulted in the formation of $^{16}O_2$ and $^{16}O^{18}O$ for a short of time in the case of MgO-based catalysts, but only marginally in the case of ZnO. Lattice oxygen of the support oxide is the only possible source of ^{16}O. Oxygen at the surface of the MgO core is exchanged, exposing simultaneously O_2 dissociation sites. Zinc oxide, however, shows almost no oxygen exchange. Thus, the mechanism of O_2 dissociation and exchange, depending on the support nature, critically determines the catalytic activity. We speculate that the differences are related to the fact that MgO forms only labile oxygen vacancies (surface defects),[14] while ZnO is easier to

dx.doi.org/10.1021/ja505411s | J. Am. Chem. Soc. XXXX, XXX, XXX−XXX

reduce, generating more stable oxygen vacancies due to lattice relaxation.[15]

Reaction Mechanism and Conclusions. Let us combine now the individual experiments to build a mechanistic hypothesis for the selective catalytic reaction pathway of the oxidative conversion of ethane to ethene, considering the proposed sequence of individual reaction steps (Schemes 1 and 2). Given the complexity of the reaction sequence we have not considered several conceivable reaction routes by excluding them via circumstantial evidence. We are aware of the presence of a steady state concentration of water in this chloride melt but did not consider its influence on the chloride properties in this contribution in other than the explicit ways discussed below.

Scheme 1. Suggested Elementary Steps of the Reaction Pathway (□: active Sites on Support; *: Active Sites on Surface of Melt)

1. $O_{2\,(g)} \rightleftharpoons O_{2\,(melt)}$
2. $O_{2\,(melt)} + \square \rightleftharpoons O_2\square$
3. $O_2\square + Cl^- \rightleftharpoons O\square + OCl^-_{(melt)}$
4. $O\square + Cl^- \rightleftharpoons OCl^-_{(melt)} + \square$
5. $OCl^-_{(melt)} \rightarrow OCl^-_{(surf.)}$
6. $C_2H_6 + OCl^-_{(surf.)} + 3\,* \rightarrow \cdot C_2H_5\,* + HCl* + O^{-*}$
7. $\cdot C_2H_5\,* + O^{-*} \rightarrow OC_2H_5^{-}\,* + *$
8. $OC_2H_5^{-}\,* \rightarrow C_2H_4 + OH^{-*}$
9. $OH^{-*} + HCl* \rightarrow H_2O + Cl^- + 2\,*$

Scheme 2. Schematic Representation of the Reaction Sequence in Ethane ODH over Supported Alkali Metal Chloride Catalysts

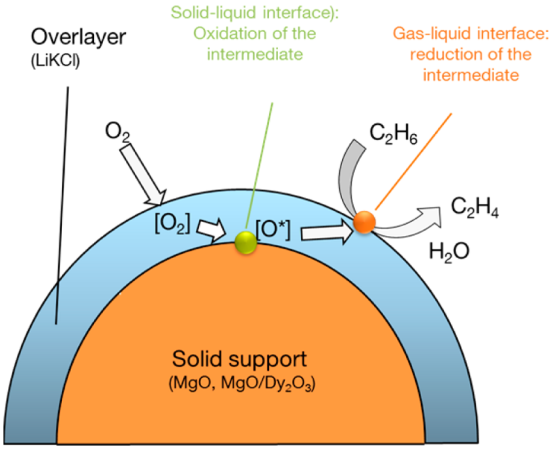

The transient formation of Cl• radicals or Cl_2 has been excluded on the basis of the absence of corresponding electron spin resonance spectroscopy signals and of the absence of even traces of chlorinated species from the product mixtures. The formation of ethyl chloride, which eliminates HCl to form ethene has been ruled out, because of the stability of the chloride catalyst, and no retention of HCl was observed when scrubbing the reactor exhaust by a caustic solution. We also ruled out significant hydrolysis of the supported chloride by the water formed in the reaction and the formation of HCl through the reaction

$$NaCl + H_2O \rightleftharpoons NaOH + HCl$$

because of the thermodynamic equilibrium of the reaction. As a consequence, we assume it to be most likely that the oxidizing species is the hypochlorite anion.

The isotope scrambling experiments show conclusively that the ODH reaction follows a Mars–van-Krevelen type mechanism with independent, but kinetically coupled steps for the activation of O_2 and ethane. Oxygen is molecularly absorbed in the polar chloride melt (Step 1). The temperature programmed exchange between labeled O_2 shows that the exchange takes place at the support surface and is kinetically hardly limited by the presence of the supported chloride. On the basis of the rapid transient (Figure 3) and the temperature programmed exchange reactions, we conclude that O_2 is quasi-equilibrated in the melt and that its concentration is low. The reactive dissociation of O_2 (Step 2) takes place at the interface between support and liquid melt.

Dissociated O_2 at the interface forms an oxygen–chlorine intermediate (Steps 3 and 4), which we currently speculate to be hypochlorite anions. These steps are concluded to be reversible, because the purge period between O_2 loading and ethane exposure decreased the concentration of the active species. It should be noted in passing that the decay followed a second order in the concentration of redox active species and that Cl species have not been detected in the gas phase. The second-order kinetics leads us to speculate that the decay is related to a reaction between two hypochlorite anions, but it is unclear whether this occurs in the melt or at the support surface. The reactive intermediate (OCl^-) diffuses throughout the molten chloride and, hence, establishes a concentration at the surface of the melt proportional to the chemical potential in the bulk and at the two interfaces (Step 5). As shown by the transient between ethene and O_2 exposure (Figure 3b), ethane is not absorbed into the polar melt. Thus, ethane activation is concluded to proceed exclusively at the surface of the melt. Ethane is hypothesized to adsorb on the surface of the melt on a hypochlorite anion, resulting in the abstraction and the formation of a subsequent C_2H_5 radical species and •O^- and HCl (Step 6). The •C_2H_5 species reacts with the •O^- species and forms a surface complex (Step 7), which is cleaved into ethene and a hydroxyl anion (Step 8). Finally, OH^- reacts with HCl forming water (Step 9). As ethane scrambling did not yield isotopically mixed ethane species, those in the latter two steps are concluded to be irreversible. The adsorbed hydrocarbon radical reacts with O^-, resulting in the formation of ethene and water via an oxidized intermediate (Steps 6 and 7). Thus, we conclude that ethane is activated at the gas-melt interface, and O_2 is activated at the melt-support interface. We attribute the outstandingly high selectivity to the separation of alkane and O_2 activation sites.

The nearly ideal selectivity for ODH of the intermediate species stored in the melt does not preclude, however, combustion initiated by gas-phase O_2. This is shown by the step experiments (Figure 3), which demonstrate that the chemically stored oxygen (in the form of an oxidizing species) is active generating ethene, but not CO_2 or CO. The SSITKA experiments additionally showed a slower O_2 isotopic exchange in the ODH pathway compared to the total oxidation pathway. Unlike many other oxidation catalysts (e.g., supported vanadia[12] or molybdena[16]) the H/D isotope effect strongly suggests that the cleavage of the first C–H bond is not involved in the rate-determining step over supported alkali chloride. In the present case, the cleavage of the O_2 bond leading to the oxidizing species appears to be the slow step. Thus, only when

dx.doi.org/10.1021/ja505411s | J. Am. Chem. Soc. XXXX, XXX, XXX–XXX

ethane collides with this oxidizing species at the surface of the melt is reaction possible.

At this point we would like to analyze the molecular consequences of the spatial separation of oxygen and ethane activation and the fact that ethane has no physical access to the oxygen activation site. Oxygen activation on metal oxide surfaces proceeds conventionally by a stepwise electron transfer placing the charge on the oxygen ion.[11] In the present case, the adsorbed surface O_2 is reduced by redox active sites acquiring a partial positive charge, while creating a partially negative charge with the formed oxygen species. A subsequent formation of the ionic oxygen species is hindered by the limited availability of electrons at the redox site being part of an isolating oxide. Low concentrations of such sites and a high barrier (approximately 200 KJ/mol) make this step kinetically slow. The oxygen activation in the supported alkali chloride system is assumed to take place near O vacancies which are likely to form in MgO surfaces.[17] Over the vacancy on MgO, O_2^- is likely to form while exposed to O_2,[18,19] known as an unselective oxygen species (Scheme 3), which would form on bare metal oxide surfaces.

Scheme 3. Possible Molecular Pathway of Chloride-Assisted O_2 Activation at MgO Oxygen Vacancies

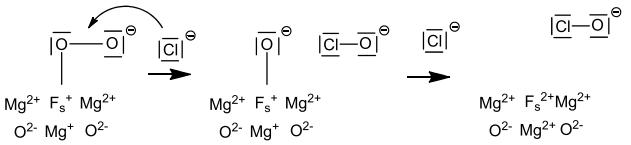

The chloride layer of the catalysts studied prevents the access of hydrocarbons to such active oxygen. The ubiquitous presence of Cl^- facilitates the formation of an oxidized chlorine species, presumably OCl^- (Scheme 3, where this process is exemplified for hypochlorite as an active species). Its anionic nature allows the chlorine−oxygen species to desorb readily from the lattice of the support (being formally replaced by Cl^-) and to diffuse in the melt. As the electrophilic oxygen species has reacted with Cl^-, the strongly electrophilic character has been reduced and an anion has been formed. The precise nature of the active oxygen intermediate remains, however, the subject of further investigation. The chlorine containing oxyanion diffuses to the surface of the melt, is stabilized there in low concentrations as isolated species, and reacts eventually with ethane. The formed ethene rapidly desorbs from the melt due to its low affinity to a highly polar and dynamically rearranging surface.

Thus, in summary, we propose a direct and a reverse Mars−van Krevelen step[20] in which ethane and O_2 are converted at different interfaces, namely the molten overlayer/gas phase and the molten overlayer/solid support interfaces, respectively. The active oxygen species is formed at the oxygen vacancies at the support, e.g., MgO in the present case, and diffuses through the chloride melt to the surface. Thus, the active oxygen species is dissolved in a molten phase and exists at the surface only in low concentrations. The species has an anionic character, but it should be emphasized that, e.g., the hypochlorite is able to assume also a radical form. Compared to the highly electrophilic oxygen formed on other typical ODH catalysts,[21] the present species react more slowly, but with less tendency to initiate total oxidation. Depending on the overlayer thickness, the concentration of active species varies in different catalysts. A continuous cover helps in increasing the concentration of sites active for the oxidative dehydrogenation (the apparent activation energy actually increases), the reactivity of catalysts decreases, as with increasing overlayer thickness the steady-state rate of formation of the oxidizing species at the surface of the support leads to a lower density in the chloride volume and on the surface.

The present system of supported chlorides offers an exciting new route toward olefins, which combines high selectivity and reasonable ethene production rates. While the positive effect of chloride for oxidative dehydrogenation had been previously established[22,23] and has even been observed in molten systems of other halogenides,[24] the current contribution shows how the interplay between the support in the chemistry in the supported chloride may direct alkane oxidative dehydrogenation to new levels. We are convinced that a further improvement of the molecular understanding of this system could lead to improvements in our current access to ethene as well as to larger and certainly more complex olefins via oxidative dehydrogenation.

EXPERIMENTAL SECTION

Catalyst Preparation. Catalysts were prepared by wet impregnation of chlorides. The support material (MgO (Aldrich, >99%), Dy_2O_3 (Aldrich, 99.9%), ZnO (Aldrich, 99.9%), or ZrO_2 (Aldrich, 99.5%)) was added to 100 mL deionized water, followed by the chloride salts forming the overlayer (LiCl (Aldrich,>99.5%)), KCl (Merck,99,5%), NaCl (Merck, puriss.), CsCl (Aldrich, >99.5%)). The slurry was stirred at 80 °C for 2 h, followed by the evaporation of water under reduced pressure. The residue was dried at 120 °C for 12 h and calcined in synthetic air (100 mL/min) at 650 °C for 12 h. Table 3 compiles the chemical compositions of the catalysts.

Table 3. Compositions of Catalysts

no.	support 1	support 2	overlayer 1	overlayer 2	support 1 [mol]	support 2 [mol]	overlayer 1 [mol]	overlayer 2 [mol]	overlayer [mol %]
1	MgO	Dy_2O_3	LiCl	KCl	0.165	0.0031	0.00129	0.000872	1.27
2	MgO	Dy_2O_3	LiCl	KCl	0.165	0.0031	0.00299	0.00293	3.40
3	MgO	Dy_2O_3	LiCl	KCl	0.165	0.0031	0.0059	0.004	5.57
4	MgO	Dy_2O_3	LiCl	KCl	0.165	0.0031	0.012	0.008	10.67
5	MgO	Dy_2O_3	LiCl	KCl	0.165	0.0031	0.0240	0.0159	19.23
6	MgO	Dy_2O_3	LiCl	KCl	0.165	0.0031	0.048	0.0321	32.23
7	MgO	Dy_2O_3	LiCl	KCl	0.165	0.0031	0.072	0.048	41.65
8	MgO	–	LiCl	KCl	0.168	–	0.0240	0.0159	19.23
9	ZnO	–	LiCl	KCl	0.168	–	0.0240	0.0159	19.23
10	MgO	Dy_2O_3	NaCl	CsCl	0.165	0.0031	0.014	0.026	19.23

dx.doi.org/10.1021/ja505411s | J. Am. Chem. Soc. XXXX, XXX, XXX−XXX

To selectively tailor surface properties of MgO, one catalyst (composition according to row 8 in Table 3) was synthesized using MgO sintered at 900 °C for 12 h in synthetic air in a muffle furnace.

Physicochemical Characterization. BET surface areas and pore size distributions were determined by N_2 adsorption−desorption at 77 K using a PMI Automated BET Sorptomatic 1900 series instrument. Prior to the adsorption, the samples were evacuated at 250 °C for 2 h.

ICP-OES. ICP-OES was performed with a SpectroFlame Typ FTMOA81A ICP-OES spectrometer from Spectro Analytical Instruments. Samples were suspended in deionized water under ultrasonic treatment. All samples were filtered before analysis.

Reactant Gases. For ODH of ethane, the following gases (all supplied from Westfalen AG) were used: He 3.5, ethane (99.995%), and O_2 (10.1%, diluted in He 3.5). For calibrations, ethene 3.5 was used. For the isotopic labeling studies, C_2D_6 and $^{18}O_2$ (97% isotope enrichment) were used.

Catalytic Tests. Catalytic tests were carried out in a plug flow reactor consisting of a catalyst fixed-bed in a quartz tube surrounded by a heat distributing block and heating coils. Most experiments used 300 mg of the catalysts diluted in 700 mg SiC (450−600 μm) to improve the heat transfer and ensure homogeneous temperature over the entire catalyst bed. Layers of SiC and quartz wool encased the catalyst bed to minimize dead volume. Reactant flow rates were individually adjusted by mass flow controllers (Bronkhorst). The effluent stream composition was quantified by a Maxum Edition II Process gas chromatograph (Siemens) equipped with TCD detectors. Oxygen, CO, and CH_4 were separated on a Molesieve 5A column (2 m, 60/80 mesh), and the hydrocarbons other than CH_4 were separated on a HayeSep Q column (2 m, 80/100 mesh) combined with a HayeSep T precolumn (0.5 m, 80/100 mesh). The time-resolved product stream analysis in transient experiments and isotopic studies was accomplished with a calibrated Pfeiffer Omni StarTM GSD 320 °C mass spectrometer system connected in parallel.

Steady-State Kinetic Measurements. Standard conditions for steady-state experiments were partial pressures of ethane (99.5%) and O_2 (10.1% in He) of 70 mbar each with balance He (99.99%) to atmospheric pressure. A temperature range between 450 and 650 °C was explored at a WHSV of 0.8 h^{-1}.

Sequential Step Transient Experiments. The catalyst was heated to the reaction temperature in He and then 10% O_2 in He was subsequently supplied for a variable time (45 min to reach equilibrium, 1 min to establish the kinetics of the intermediate formation in a different experiment). The probe reaction with ethane (10% C_2H_6 in He) followed a purge with 40 mL/min He of variable duration detecting the ethane consumption and ethene formation by MS analysis.

Ethane and ethene were quantified by linear deconvolution of different MS signals m/z = 26, 27, 28, 29, 30.

Steady State Isotope Transient Kinetic Analysis (SSITKA). The LiKCl/MgO + Dy_2O_3 catalyst was used for the SSITKA experiment. Three hundred mg of catalyst diluted with 700 mg SiC was used at steady state for 48 h to achieve stable conversion levels. Experiments were performed at 550, 600, and 625 °C subsequent to a 20 min He purge at each temperature (Figure 5). The reaction was run at a WHSV of 0.8 h^{-1} using partial pressures 70 mbar of ethane and O_2 with He balance to atmospheric pressure. Steady state operation was established using a feed containing $^{16}O_2$ for 30 min. The influent was switched in a step function to a feed containing an identical concentration of $^{18}O_2$ instead of $^{16}O_2$, replacing additionally a small fraction of He by the inert tracer Kr. The isotope transient at steady-state was monitored for 40 min. A blank experiment at 625 °C with SiC was used to exclude contributions of gas-phase reactions. The effluent composition was quantified by MS analysis assigning the following components to the respective mass to charge ratios: $^{16}O_2$ (m/z: 32), $^{16}O^{18}O$ (m/z: 34), $^{18}O_2$ (m/z: 36), $H_2{}^{16}O$ (m/z: 18), $H_2{}^{18}O$ (m/z: 20), $C^{16}O_2$ (m/z: 44), $C^{16}O^{18}O$ (m/z: 46), $C^{18}O_2$ (m/z: 48), Kr (m/z: 84).

Isotope Scrambling Experiments. Temperature programmed isotopic exchange experiments with oxygen isotopes were performed with several catalysts. Three hundred mg catalyst was diluted with 700 mg of SiC. After preheating in He to 450 °C and a short equilibration in the O_2 isotope mixture, the temperature was increased with 5 °C/min to 650 °C, feeding a gas stream of 10 mL/min with a composition of 2.5% $^{18}O_2$, 2,5% $^{16}O_2$ and 95% He. The temperature was held at 650 °C for 15 min. $^{18}O_2$ with 97% isotopic enrichment was used. For detection of the different oxygen species, the following m/z signals were used: 32 for $^{16}O_2$, 34 for $^{16}O^{18}O$ and 36 for $^{18}O_2$.

For the case of ethane, a gas flow of 9 mL/min He, 0.5 mL/min C_2H_6 and 0.5 mL C_2D_6 was fed. The experiment was started at 450 °C with a temperature ramp of 10 K/min up to 650 °C. The signals at m/z 30, 31, 32, 33, 34, 35, and 36 were recorded.

■ ASSOCIATED CONTENT

Ⓢ Supporting Information

Several figures describing reaction kinetics and physicochemical characterization. This material is available free of charge via the Internet at http://pubs.acs.org.

■ AUTHOR INFORMATION

Corresponding Author

Johannes.lercher@ch.tum.de

Notes

The authors declare no competing financial interest.

■ ACKNOWLEDGMENTS

Funding of this research by SOLVAY as well as fruitful exchanges with Dr. Michel Strebelle, Dr. Armin Liebens, Dr. Marco Piccinini, and Paul Degraeve are acknowledged. We thank Pinghong Xu and Prof. Nigel Browning (UC Davis, PNNL) for HAADF-TEM measurements. We also thank Prof. Andreas Jentys and Maximilian W. Hahn, Technische Universität München, and Prof. Angeliki Lemonidou, Aristoteles University of Thessaloniki, for fruitful discussions. Christian Gärtner thanks the TUM Graduate School and the Department Graduate Center Chemistry.

■ REFERENCES

(1) Zimmermann, H.; Walzl, R. *Ullmann's Encyclopedia of Industrial Chemistry*; Wiley-VCH Verlag GmbH & Co. KGaA: Weinheim, 2000.

(2) Blasco, T.; Galli, A.; Lopez Nieto, J. M.; Trifiro, F. *J. Catal.* **1997**, *169*, 203.

(3) Ciambelli, P.; Lisi, L.; Pirone, R.; Ruoppolo, G.; Russo, G. *Catal. Today* **2000**, *61*, 317.

(4) Gärtner, C. A.; van Veen, A. C.; Lercher, J. A. *ChemCatChem* **2013**, *5*, 3196.

(5) Kumar, C.; Gaab, S.; Müller, T.; Lercher, J. *Top. Catal.* **2008**, *50*, 156.

(6) Tope, B.; Zhu, Y.; Lercher, J. A. *Catal. Today* **2007**, *123*, 113.

(7) Landau, M. V.; Gutman, A.; Herskowitz, M.; Shuker, R.; Bitton, Y.; Mogilyansky, D. *J. Mol. Catal. A: Chem.* **2001**, *176*, 127.

(8) Chin, Y.-H.; Buda, C.; Neurock, M.; Iglesia, E. *J. Am. Chem. Soc.* **2011**, *133*, 15958.

(9) Cherginets, V. L.; Demirskaya, O. V.; Rebrova, T. P. *J. Chem. Thermodyn.* **2004**, *36*, 115.

(10) Campbell, S.; Hollins, P.; McCash, E.; Roberts, M. W. *J. Electron Spectrosc. Relat. Phenom.* **1986**, *39*, 145.

(11) Grzybowska-Swierkosz, B. *Top. Catal.* **2000**, *11−12*, 23.

(12) Argyle, M. D.; Chen, K.; Bell, A. T.; Iglesia, E. *J. Phys. Chem. B* **2002**, *106*, 5421.

(13) Chen, K.; Iglesia, E.; Bell, A. T. *J. Catal.* **2000**, *192*, 197.

(14) Sterrer, M.; Fischbach, E.; Risse, T.; Freund, H.-J. *Phys. Rev. Lett.* **2005**, *94*, 186101.

(15) Carrasco, J.; Lopez, N.; Illas, F. *Phys. Rev. Lett.* **2004**, *93*, 225502.

(16) Chen, K.; Iglesia, E.; Bell, A. T. *J. Phys. Chem. B* **2000**, *105*, 646.

(17) Myrach, P.; Nilius, N.; Levchenko, S. V.; Gonchar, A.; Risse, T.; Dinse, K.-P.; Boatner, L. A.; Frandsen, W.; Horn, R.; Freund, H.-J.; Schlögl, R.; Scheffler, M. *ChemCatChem* **2010**, *2*, 854.
(18) Ferrari, A. M.; Pacchioni, G. *J. Phys. Chem.* **1995**, *99*, 17010.
(19) Ferrari, A. M.; Pacchioni, G. *J. Chem. Phys.* **1997**, *107*, 2066.
(20) Mars, P.; van Krevelen, D. W. *Chem. Eng. Sci.* **1954**, *3*, 41.
(21) Heracleous, E.; Lemonidou, A. A. *J. Catal.* **2006**, *237*, 175.
(22) Gaab, S.; Find, J.; Mueller, T. E.; Lercher, J. A. *Top. Catal.* **2007**, *46*, 101.
(23) Wang, D. J.; Rosynek, M. P.; Lunsford, J. H. *J. Catal.* **1995**, *151*, 155.
(24) Adams, C. T.; Brandenberger, S. G.; DuBois, J. B.; Mill, G. S.; Nager, M.; Richardson, D. B. *J. Org. Chem.* **1977**, *42*, 1.

dx.doi.org/10.1021/ja505411s | *J. Am. Chem. Soc.* XXXX, XXX, XXX−XXX